arXiv:0711.3443v3 [nucl-ex] 7 Oct 2008

Upgrade of the Glasgow photon tagging spectrometer for Mainz MAMI-C.

J.C. McGeorge[1], J.D. Kellie[1], J.R.M. Annand[1], J. Ahrens[2], I. Anthony[1], A. Clarkson[1], D.J. Hamilton[1], P.S. Lumsden[1], E.F. McNicoll[1], R.O. Owens[1], G. Rosner[1], and A. Thomas[2]

[1] Department of Physics and Astronomy, University of Glasgow, Glasgow G12 8QQ, Scotland, UK

[2] Institut für Kernphysik, Universität Mainz, D-55099 Mainz, Germany

Abstract. The Glasgow photon tagging spectrometer at Mainz has been upgraded so that it can be used with the 1500 MeV electron beam now available from the Mainz microtron MAMI-C. The changes made and the resulting properties of the spectrometer are discussed.

PACS. 29.40.Mc Scintillation detectors – 29.30.Dn Electron spectroscopy

1 INTRODUCTION

The Glasgow photon tagging spectrometer [1,2] installed at the MAMI-B 883 MeV electron microtron [3,4,5] at Mainz, Germany in 1991 has been used in many successful photonuclear experiments. The main focal plane detector [2] consisting of 353 plastic scintillators covered a tagged photon energy range of ∼40 - 820 MeV at full MAMI-B energy and allowed a maximum tagged photon flux of ∼5×10⁵ per MeV · s. Although the intrinsic resolution of the spectrometer was ∼0.1 MeV [1] the effective resolution was ∼2 MeV due to the widths of the detectors. Improved resolution over part of the energy range was provided by

a 96-element focal plane microscope [6]. Using an aligned diamond radiator tagged photons with linear polarisation greater than 45% have been produced [7,8,9,10,11] over an adjustable part of the energy range up to ∼400 MeV. Circularly polarised tagged photons were also generated using polarised electrons from MAMI-B [12]. Several powerful detector systems such as Daphne [13], CATS [14], PIP/TOF [15], TAPS [16] and most recently the Crystal Ball [17] have been used in conjunction with MAMI-B and the Glasgow tagger to make measurements on meson photoproduction and to study photonuclear reactions. Examples include studies of the Gerasimov-Drell-Hearn sum

rule [18], the E2/M1 ratio in the N $\rightarrow \Delta$ transition [19] and two nucleon knockout with linearly polarised photons [20].

The recent upgrade of the MAMI accelerator to 1500 MeV, in principle, gives access to interesting tagged photon experiments at higher energy. The photon linear polarisation can also be improved to >60% up to ~800 MeV by using the tighter collimation allowed by the smaller opening angles in the Bremsstrahlung process at higher energy. Examples of such experiments are the detailed study of the second resonance region with complete measurements on pseudoscalar meson production, rare η decay modes to look for physics beyond the standard model and strangeness production near threshold to test chiral perturbation theory. But, as the maximum attainable magnetic field in the original spectrometer was not sufficient to handle an electron energy of 1500 MeV, major modifications were necessary. This paper describes these modifications and the resulting properties of the upgraded spectrometer.

2 AIMS OF THE UPGRADE

The original spectrometer deflected the 833 MeV electron beam through ~79^0 into a beam dump recessed into the wall of the experimental hall, and the tagged photons passed into a large well shielded experimental area. It was decided, as far as possible, to preserve the original layout and also the original spectrometer optics which govern the excellent and well understood performance. This in turn avoided the costly redesign of the focal plane detector and

its mounting frame. In consequence the magnetic field in the spectrometer had to be increased from 1.0 to ~1.8 T in order to deflect the 1500 MeV beam into the original beam dump.

The original focal plane scintillators and electronics were, however, replaced since the light output had become reduced, typically by a factor greater than 10, due to radiation damage and the original electronics had become obsolete and incompatible with the CATCH [21] electronics used with the Crystal Ball detector system. As the detector geometry was not changed the effective resolution becomes ~4 MeV when tagging at 1500 MeV.

3 UPGRADE OF THE SPECTROMETER MAGNET

The existing power supply and cooling arrangements for the magnet coils allowed for a current up to 440 amps which produced a field of 1.4 T [1]. Simple estimates suggested that 1.8 T could be obtained by reducing the pole gap as long as the iron in the return yoke was increased in thickness to prevent saturation. Reducing the pole gap is permissible since angles associated with the Bremsstrahlung process scale approximately as 1/energy, and a reduction from 50 mm (for 883 MeV) to 25 mm (for 1500 MeV) does not appreciably increase the fraction of the post-Bremsstrahlung electrons (tagging electrons) which hit the pole faces of the magnet. With a 25 mm pole gap and 110 mm extra return yoke thickness (Fig 1), calculations using the finite element code TOSCA [22] showed that an

average field of $\sim$1.96 T would be reached with a current of 440 amps. Therefore new additional top, bottom and back yokes were fabricated, each of thickness 110 mm.

Measurements [1] had shown that the maximum pole gap distortion in the original spectrometer was 0.14 mm at a field of 1.0 T, and this could be expected to increase to $\sim$0.54 mm at 1.96 T. Some estimates of the stresses and distortions involved were made by finite element modelling (FEM) of the original and upgraded spectrometers as solid structures using the IDEAS [23] and ABAQUS [24] programs. The upgraded spectrometer was strengthened by replacing the main load carrying bolts with through-rods (Fig 1) fitted with special nuts which allow a controlled pre-tension to be applied by pneumatic means.

To reduce the pole gap, 12.5 mm thick shim plates (Fig. 2) were fabricated. The input and all output edges were cut at an angle of 36.1^0 to continue the chamfer of the existing poles. The shims were fixed to the poles by 129 M8 screws.

The new magnet parts were all manufactured from low carbon steel (S275). Although this has a somewhat inferior B/H curve compared to the material (AME2SX1) used in the original spectrometer, it is not very different in the region above 1.5 T. B/H curves were measured (by the Woolfson Centre for Magnetics Technology, Cardiff, UK) for samples of the material used to make the new parts and input to TOSCA to estimate the magnetic field.

The vacuum box was modified to provide a larger aperture for the two NMR probes required to cover the extended field range and also to increase the acceptance of the spectrometer to $\sim$100 milliradians in the horizontal plane. This is useful for Møller polarimetry which can be used to measure the electron beam polarisation.

In the upgraded spectrometer the maximum pole gap distortion at full current was found to be $\sim$0.42 mm. This is slightly less than predicted from scaling up the distortion measured in the original spectrometer and suggests that the through-rods had a beneficial effect.

The photon collimator was re-aligned on the input beam direction with an accuracy of $\sim$0.2 mm using the adjustments built into the V-shaped collimator mounting block. The focal plane detector support structure is fixed to the magnet, but it was surveyed to check that it was remounted in the same position as before to an accuracy of about 1 mm.

4 MAGNETIC FIELD MEASUREMENTS

Calculations of the magnetic field in the upgraded spectrometer made with TOSCA indicated that the field would become more non-uniform as the field is increased. As a result the energy of the tagging electrons, expressed as a fraction of the incident beam energy, reaching a particular position in the focal plane is expected to change slowly as the beam energy increases. The spectrometer resolution should be less affected since the opening angle of the tagging electrons is small. Since both the energy calibration and the energy resolution of the spectrometer can be measured using electron beams of accurately known energy from MAMI, complete field maps of the upgraded spectrometer at several fields were not made. However some

field measurements were made using a temperature compensated Hall probe which had been calibrated against an NMR system. The field measured at mid-pole gap along line Bb in Fig. 2 is shown in Fig. 3. It can be seen that the measured field at 435 amps comfortably exceeds the 1.8 T required to handle 1500 MeV. It is in good agreement with the TOSCA prediction, both at the edge from which the electrons exit and in the central region, except for the 'dips' at positions 25.5 and 42.5 cm corresponding to the locations of two of the M8 screws which secure the pole shims. Similar results were found along lines Aa and Cc.

It is not clear whether the 'dips' are predominantly due to saturation of the screw material or to the missing metal which arises from the clearance at the end of the tapped holes. Measurements over a few screws indicate that the field reduction has a peak value of $\sim3.0\%$ and a full width at half maximum of about 17.5 mm. Again, the effect on the energy resolution is expected to be small but there will be local deviations from a smooth energy calibration. This is discussed in Sect. 6.

It was not possible to re-optimise the field clamps for the reduced pole gap without large scale mechanical reconstruction, and the effect on the field edge was therefore examined carefully. Both the field measurements and the TOSCA calculations indicate (Fig. 3) that in the upgraded spectrometer the field edge is displaced inward from the physical pole edge (see Fig.4 in ref [1]). This was quantified by determining the effective field boundary (EFB) position for five locations based on the field calculated

using TOSCA. The EFB position was found by making the field integrals, $\int B.dl$, equal for the uniform and calculated fields along lines perpendicular to the pole edge, where the magnitude of the uniform field is taken to be the average field calculated for the region 100-200 mm inside the physical pole edge. The EFB's were found to be 21 ± 1 mm inside the physical boundaries along lines Aa, Bb and Cc in Fig. 2.

5 FOCAL PLANE DETECTOR

5.1 The detectors

The focal plane (FP) of the tagger dipole magnet is instrumented (see Fig. 2 and Figs. 1 and 3 in ref [2]) with 353 overlapping plastic scintillators which cover an energy range of around 5 - 93% of E_0, the energy of the primary electron beam. The scintillators are mounted in milled slots to define their positions and angles with respect to the tagging electrons, which are momentum analysed by the dipole magnet. The scintillators have a length of 80 mm, a thickness of 2 mm and widths of 9 to 32 mm. These decrease along the focal plane in order to keep the tagged energy range covered by each detector roughly constant. The scintillator strips overlap by slightly more than half their width (see Fig. 3 in ref [2]) so that an electron hit is defined by coincident signals in adjacent detectors. The width of the overlap region (a 'channel') is equivalent to an energy width of ~4 MeV, for an incident electron beam energy of 1500 MeV, and neighbouring channels overlap by about 0.4 MeV.

The scintillator EJ200 was chosen for the refurbishment because the scintillation spectrum better matches the response of the phototube and it is thought to be less susceptible to radiation damage than the slightly faster NE 111/Pilot U used in the original setup. The 353 new scintillators were glued, using ultra-violet curable epoxy, to new light guides made from acrylic which has good transmission at blue to near ultra-violet wavelengths. They were then wrapped in double-sided, aluminised Mylar to eliminate optical cross talk and mounted in the original detector frame [2].

Before installation about half of the scintillators were tested using a Sr90 source and the signal amplitude was found to decrease linearly with increasing width. Compared to the old detectors, the new scintillators produced one to two orders of magnitude more light, due mainly to radiation damage accumulated by the former in around 15 years of service.

5.2 Photomultiplier amplifier-discriminator electronics

Each scintillator on the FP is fitted with a Hamamatsu R1635 photomultiplier tube (PMT). As the PMTs are affected by stray fields of more than $\sim$0.01 T, 0.2 mm thick mild steel plates were fitted along the whole length of the detector array on either side of the PMTs. Together with the standard cylindrical μ-metal screens fitted to every PMT, this was found to be sufficient to cope with the increased stray field from the upgraded magnet when operated at maximum field.

Most of the original PMTs are still in good working order. A total stock of around 450 was sorted on the basis of gain, with the highest gain tubes fitted to the low-momentum end of the spectrometer, grading progressively down in gain along the length of the focal plane. This partially compensates for the less efficient light collection from the relatively broad scintillators at the high-momentum end.

Every PMT is attached to a custom designed amplifier-discriminator (A/D) card (Fig.4). High voltage (HV) is distributed to the PMT electrodes through a Zener stabilised base chain which may be operated from $900 - 1500$ V. Typically a PMT is run at around -1100 V, drawing a current of around 0.3 mA, while each A/D card draws $\sim$370 mA from the +5 V and $\sim$250 mA from the -5 V LV supply lines.

The anode signal is amplified by a factor 10 and fed to a dual, low-high threshold discriminator which supplies a LVDS-logic signal to drive TDCs and scalers. The differential LVDS signal is transported on $\sim$10 m of 0.05"-pitch cable, to active fanout cards which connect to sampling, multi-hit TDCs and scalers (designated CATCH). These were originally designed [21] for the COMPASS experiment at CERN. The sampling TDCs, which have a channel width of 0.117 ns and double pulse resolution of 20 ns, remove the need for delay in the TDC input lines, which was necessary in the original setup to accommodate the delay in the trigger system. The fine-pitch cable, which is commonly used to connect SCSI-bus peripherals, is much less bulky than standard 0.1" pitch cable and, over a 10 m

length, produces no significant degradation of edge speed in the 10 ns wide pulse. In the previous implementation of the tagger electronics, pulse widths had to be at least 20 ns to drive the ~100 m of delay cable before the TDC input. An active logic fanout is necessary not only to drive CATCH modules, which cannot be "daisy-chained", but also for auxiliary ECL-logic electronics, such as used to select Møller-scattering events for electron-beam polarisation analysis.

The ×10 amplified anode signal, produced by illumination of the R1635 PMT photocathode by a 1 ns duration diode laser, is displayed in Fig. 5. The amplifier produces no discernible degradation of edge speed and the 10-90% rise time is 1.9 ns. This output also connects, via a ×1.3 buffer stage and a coaxial delay line, to a LeCroy 1885F FASTBUS QDC which is normally read out during HV adjustment to align FP detector gains.

5.3 Detector performance

The performance of the FP detectors and electronics is illustrated in Fig. 6 which displays spectra taken with the MAMI-C 1508 MeV electron beam incident on a 10 micron thick Cu radiator. Bremsstrahlung photons, detected by a lead-glass Cherenkov detector placed directly in the beam, triggered the data acquisition system and provided gates for the charge integrating QDCs and the time reference for the TDCs.

The upper plot shows the pulse height spectrum produced by the tagging electrons in a single FP detector. This has very little background below the Landau distri-

bution showing that detector noise levels are well below the minimum ionising signal. It also suggests that any uncharged background, for example from electron-beam interactions with beam-line components is suppressed very effectively.

The lower plot of Fig. 6 shows the difference in hit times for two adjacent FP channels when an electron passes through the small region where the channels overlap. The time variation of the lead-glass trigger cancels in this difference so that the observed width of the distribution for elements i and $i+1$ is $\delta t \simeq \sqrt{\delta t_i^2 + \delta t_{i+1}^2}$, where δt_i is the timing uncertainty for element i. Assuming $\delta t_i \simeq \delta t_{i+1}$, the Gaussian-fit width (σ) of 0.24 ns is equivalent to a single-counter resolution of 0.17 ns (0.40 ns FWHM). This performance is fairly typical, with measured single-counter widths in the range 0.37 - 0.53 ns (FWHM) and is significantly better than the pre-upgrade system where the best performance obtained was ~1ns FWHM.

6 TAGGER ENERGY CALIBRATION

In the analysis of an experiment with the tagger it is necessary to know the energy of the tagging electrons which hit the centre of each focal plane detector channel. As the MAMI beam energy can be measured with an uncertainty of 140 keV [25] the tagger calibration can be carried out directly using very low current MAMI beams of lower energy than in the main experiment. However, it is only practical to obtain a small number of calibration points in this way.

In the measurement the MAMI beam is 'scanned' across several (typically 12) focal plane detectors by varying the tagger field slightly (up to $\pm 5\%$) around the value required to dump the beam correctly in normal tagging (eg. around 1.834 T which is used when tagging with 1508 MeV). By making fine steps it is possible to measure the field values for which the beam hits the small overlap regions (see Sect. 5.1) between neighbouring channels. This gives the hit position to an accuracy of about ± 0.05 channel. Interpolation of channel number versus field then gives the (fractional) channel number hit for the correct field (1.834 T in the above example). Such calibration measurements have been made with MAMI energies 195.2, 405.3, 570.3, 705.3 and 855.3, for a field of 1.057 T (which is used to dump 833 MeV in normal tagging) and for a field of 1.834 T where MAMI energies of 1002.3 and 1307.8 MeV were also used. The resulting calibration for 1.834 T is shown in the upper part of Fig. 7 and compared to that calculated assuming a uniform field as described below. The difference between the measured and calculated calibration is shown in the lower part of the figure.

If the field shape along any electron trajectory were independent of field magnitude, it would be possible to 'simulate' intermediate tagging electron energies, E'= EB/B' by varying the tagger field (B') away from the field B for which the spectrometer is being calibrated using MAMI energy E. The error that arises because the field shape is not independent of field magnitude was investigated by making several overlapping scans using different beam energies. It was found that the error is too large for this method to provide useful extra calibration information unless a suitable correction can be applied. While the assumption that the required correction is a linear function of B-B' is thought to be sufficiently accurate over the small energy range required for calibration of the microscope detector (see ref [6]), it may not be reliable over the wider range required to provide extra, widely spaced, calibration points. Therefore the calibrations were based only on the seven (or five) points measured with the seven (or five) different energies from MAMI at the correct field of 1.834 T (or 1.057 T). To guide the interpolation between these points a computer program has been written to calculate the calibration on the basis of a uniform tagger field with the effective field boundary determined in Sect. 4. The relative positions and angles of the scintillators are known from the construction of the support frame [2] and its position relative to the magnet was determined by surveying. For electron trajectories made up of circular arcs and straight lines the required calibration can be calculated by simple geometry. The strength of the field is taken from the value measured using a Drusche NMR system multiplied by a factor, f, which accounts for the difference between the field at the NMR probe (see Fig. 2) and the average field encountered by the tagging electrons. The value of f was adjusted to fit the measured calibration points.

For 1508 MeV the calculated calibration is within about 1.5 MeV of the measurements over most of the energy range (lower part of Fig. 7) but the discrepancy increases to about 4 MeV for the lowest photon energies. This be-

haviour is thought to be due to the large-scale non-uniformity of the field that can be seen partly in Fig. 3. As the effect varies smoothly over the tagged energy range the required correction to the uniform field model prediction can be obtained by fitting a smooth line to the seven points in the lower part of Fig. 7.

Similar results have also been obtained for a field of 1.057 T. The value of f was found to be 1.0098 for 1.057 T and 1.0003 for 1.834 T.

The deviations from a smooth calibration caused by the field dips due to the pole shim mounting screws (see Sect. 4) have been investigated. Estimated shifts (along the focal plane) of the tagging electron trajectories brought about by the field dips are shown in Fig. 8 as a function of the tagging electron energy, E, expressed as a fraction of the main beam energy, E_0. This estimate was obtained by assuming the field is uniform between the poles (except for the 'dips') and zero elsewhere and then calculating the total effect on exit position and bend angle caused by all dips whose centre is within 30 mm of the tagging electron trajectory. It is assumed that the fractional effect on bend angle is simply the fractional deficit in the field integral compared to that for a uniform field with no dips. The peaks in Fig. 8 occur when the electron trajectory passes over or near the centre of one or more M8 screws. For example, as can be seen in Fig. 2, one screw near the output edge lies near the $E/E_0 = 0.18$ trajectory, and 3 screws lie on or close to the $E/E_0 = 0.41$ trajectory.

The line in Fig. 8 shows the result of smoothing the shifts and values at the peaks and valleys are typically ±0.6 mm different from this line. Although the trajectory shifts due to the 'dips' in the real field may be different in detail from this simple estimate, Fig. 8 implies that the error that results from using a calibration method where the calibration is assumed to be smooth is about ±0.2 MeV when tagging with a main beam energy of 1500 MeV. This is small compared to the 4 MeV channel width of the main focal plane detector. However it may be significant in experiments which use the focal plane microscope [6] where the channel width is ∼2 mm along the focal plane. In such experiments a detailed energy calibration can be performed by using one or two different electron beam energies from MAMI and 'scanning' them across the microscope by making small variations in the magnetic field in the spectrometer (see ref [6]).

Such a scan can also be used to look for the effects of the shifts predicted in Fig. 8 over the small range covered by the microscope detector. This has been done with the microscope covering the range $E/E_0 = 0.27$ - 0.35 (indicated by the horizontal bar in Fig. 8). In Fig. 9 the measured microscope calibration points are compared to the calibration calculated assuming a uniform field and using the known microscope geometry. As the microscope position and angle were not known with sufficient precision these were adjusted in the calculation to fit the measured points. The difference between the measured points and the calculation is shown in detail in Fig. 10. The line in this figure shows the difference between the original points and smoothed line in the relevant section of Fig 8. The agreement in Fig 10 is good enough to give some confidence

in the estimate, made above, of the energy calibration error arising from the assumption that the calibration is smooth.

Including the uncertainty in the MAMI beam energy the uncertainty in the seven calibration points (measured for tagging at a main beam energy of 1508 MeV) is estimated to be about ± 0.3 MeV. Measurements of the pole shim thicknesses suggest that small variations in the pole gap could cause slight structure in the calibration between the measured points. Including this, it is estimated that the error in the calculated calibration, after correction for large-scale field non-uniformity using the fit shown in the lower part of Fig. 7, is about ± 0.5 MeV for channels up to ~ 270. It could be significantly larger for lower tagged photon energies where the shape of the correction is less well defined. There is also an additional uncertainty caused by the field dips. From Fig 8, this is estimated to be typically about ± 0.2 MeV.

7 THE PERFORMANCE OF THE UPGRADED SPECTROMETER

The intrinsic resolution of the upgraded spectrometer was measured at a field of 1.95 T which made an 855 MeV beam from MAMI hit the microscope detector placed near the middle of the focal plane. Multiple scattering in a 2 mm thick Al sheet placed in the beam at the radiator position was used to simulate the opening angle distribution of tagging electrons. From the distribution of electrons hitting a small number of microscope channels the resolution

was found to be ~ 0.4 MeV FWHM. This is an overestimate because the opening angles in this test were about 3 times bigger than is the case for the tagging electrons from a typical radiator at 1508 MeV main beam energy. It shows that when the main focal plane detector is used its channel width (~ 4 MeV) dominates the tagged energy resolution. For some experiments which make use of the focal plane microscope, however, it may be necessary to make more careful measurements of the resolution.

Measurements of the 'tagging efficiency', that is the fraction of the tagged photons which pass through the collimator, were made at reduced beam current using a 25 cm^3 lead-glass Cherenkov detector placed on the photon beam line. The results from a measurement using a 10 micron thick Cu radiator and a 4 mm diameter collimator are shown in Fig. 11. The measured tagging efficiency was found to be significantly smaller than predicted by a Monte Carlo calculation which includes the input beam divergence and diameter, multiple scattering in the radiator, the Bremsstrahlung photon opening angle distribution and the effect of Møller electron scattering. A similar discrepancy was also found using a collimator diameter of 3 mm and a 6 micron thick Ta radiator. Although not fully understood, much of the discrepancy may be due to slight misalignment of the collimator. The measured tagging efficiency is, however, stable and reproducible. Measurements made several months apart averaged over all tagger channels agree to better than 1%.

As a test of the focal plane detector background, the count rate was measured with no radiator in the beam.

It was found to be about 5×10^{-5} times smaller than the rate with a 10 micron thick Cu radiator in the beam.

The maximum useful tagged-photon intensity depends on the maximum rate at which the FP counters can be run. Up to a rate of ∼1 MHz per channel (detector singles rate of ∼2 MHz) no major change of pulse height was observed, so that the detection efficiency for minimum ionising particles did not change significantly.

Tests using a 30 micron thick diamond radiator and a 1 mm diameter collimator have been done to check that the upgraded system can produce linearly polarised photons. The tagger spectrum observed in coincidence with a Pb glass detector placed in the photon beam is shown in Fig. 12. The diamond angles were set so that the main coherent peak is at a photon energy of 680 MeV. From the height of the coherent peak above the incoherent background the degree of linear polarisation in the peak channels is seen to be ∼65% (after taking account of the fact that the coherent radiation is not 100% polarised by making use of equations 108 in ref [8]).

8 SUMMARY

The upgrade of the Glasgow photon tagging spectrometer at Mainz has been completed successfully. When used with the 1508 MeV beam from MAMI-C and the main focal plane detector it provides tagged photons in the energy range 80-1401 MeV with a photon flux up to $\sim 2.5 \times 10^5$ photons per MeV and energy resolution of ∼4 MeV. Energy calibration has been made using the accurately known MAMI energies.

The upgraded spectrometer has been in regular use for tagged-photon experiments with the Crystal Ball and TAPS since the beginning of 2007, using incident energies of 883 MeV and 1508 MeV. Experiments to investigate η and K meson photoproduction on the proton have already yielded very promising preliminary results and will continue with various polarised and unpolarised targets.

References

1. I. Anthony, J.D. Kellie, S.J. Hall and G.J. Miller, Nucl. Instr. and Meth. **A301** (1991) 230.

2. S.J. Hall, G.J. Miller, R. Beck and P. Jennewein, Nucl. Instr. and Meth. **A368** (1996) 698.

3. H. Herminghaus, K.H. Kaiser and H. Euteneuer, Nucl. Instr. and Meth. **A138** (1976) 1.

4. T. Walcher, Prog. Part. Nucl. Phys. **24** (1990) 189

5. J. Ahrens et al., Nuclear Physics News **4** (1994) 5.

6. A. Reiter et al., Eur. Phys. J. **A30** (2006) 461.

7. D. Lohman et al., Nucl. Instr. and Meth. **A343** (1994) 494.

8. U. Timm, Fortschritte der Physik **17** (1969) 765.

9. F. Rambo et al., Phys. Rev. **C58** (1998) 489.

10. F.A. Natter, P. Grabmayr, T. Hehl, R.O. Owens and S. Wunderlich, Nucl. Instr. and Meth **B211** (2003) 465.

11. K. Livingston, 'The Stonehenge Technique: a New Method of Crystal Alignment for Coherent Bremsstrahlung Experiments', International Conference on Charged and Neutral Particle Channeling Phenomena, Frascati (2005) 170.

12. K. Aulenbacher, Nucl. Instr. and Meth. **A391** (1997) 498.

13. G. Audit et al., Nucl. Instr. and Meth. **A301** (1991) 473.

14. F. Wissmann et al., Phys. Lett. **B335** (1994) 119.

15. I.J.D. MacGregor et al., Nucl. Instr. and Meth. **A382** (1996) 479, P. Grabmayr et al., Nucl. Instr. and Meth. **A402** (1998) 85.

16. R. Novotny, IEEE Trans. Nucl. Science, **38** (1991) 379.

17. M. Oreglia et al., Phys. Rev. **D25** (1982) 2259, S. Starostin et al., Phys. Rev.**C64** (2001) 055205.

18. J. Ahrens et al., Phys. Rev. Lett. **87** (2001) 02203.

19. R. Beck et al., Phys. Rev. Lett. **78** (1997) 606.

20. C.J.Y. Powrie et al., Phys. Rev. **C64** (2001) 034602, S. Franczuk et al., Phys. Lett. **B450** (1999) 332.

21. A common readout driver for the COMPASS experiment, T. Schmidt, Ph.D. thesis, Albert-Ludwigs-Universität, Freiburg, May 2002.

22. A.G.A.M Armstrong, C.P. Riley and J. Simkin, TOSCA: 3D Static Electromagnetic/Electrostatic Analysis Package, RL-81-070 (Rutherford Appleton Laboratory, 1982), TOSCA: 3D Magnetic Field Computation (Vector Fields Ltd., 24 Bankside, Kidlington, Oxford, UK.)

23. SDRC Inc., Cincinnati, Ohio, USA.

24. Hibbett, Karlsson and Sorenson Inc., Pawtucket, Rhode Island, USA.

25. K.-H. Kaiser, private communication, A. Jankoviak et al., Eur. Phys. J. A direct (2006) DOI: 10.1140/epja/i2006-09-016-3.
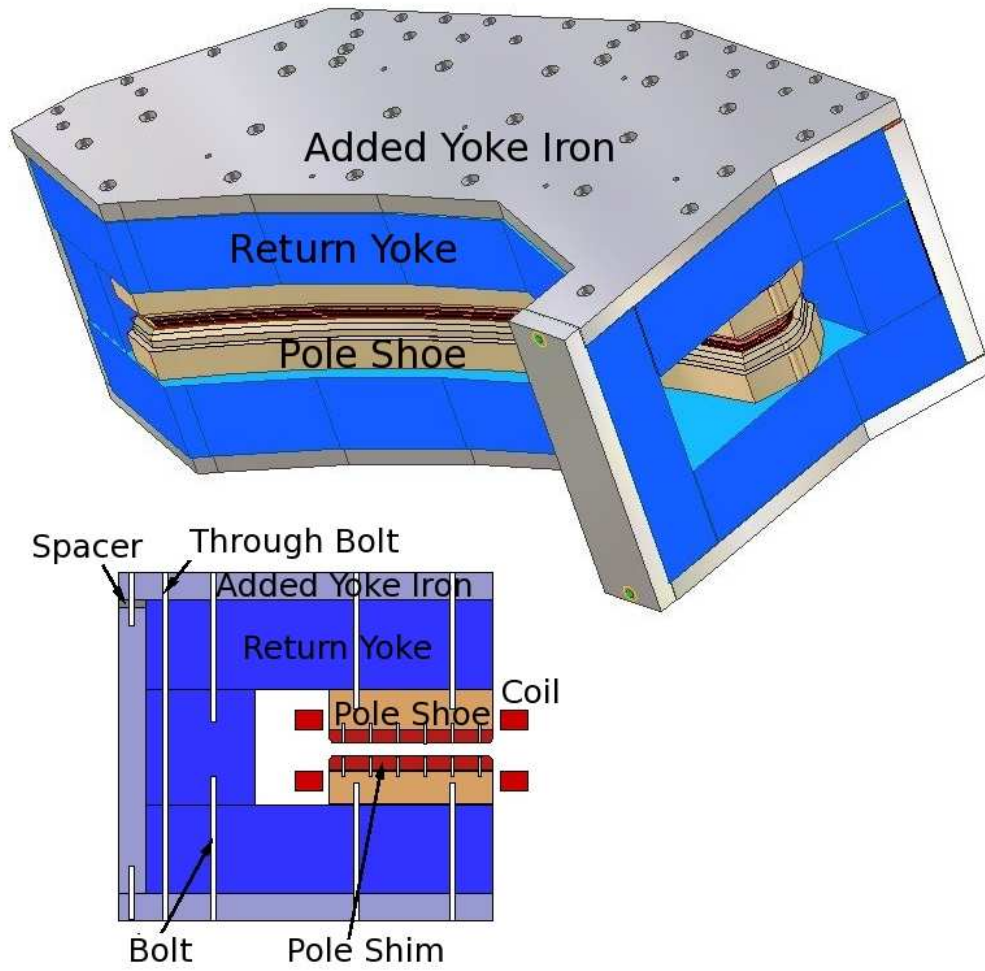
Fig. 1. The upgraded photon tagging spectrometer - 3D view (upper) and cross section (lower).
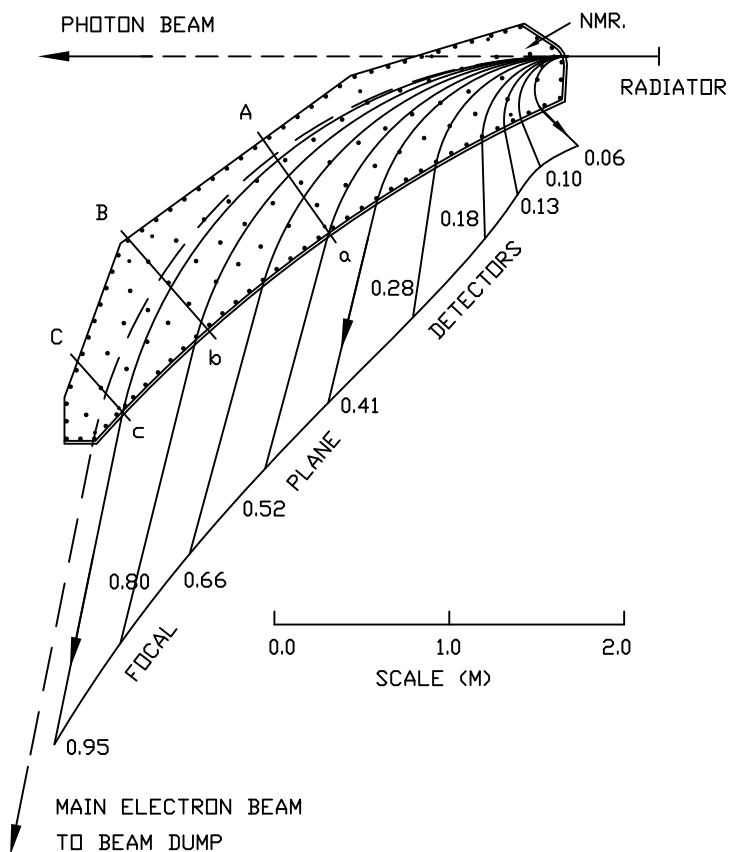
Fig. 2. Plan drawing of the lower pole shim (the upper pole shim is similar) showing the locations of the M8 screws which fix it to the pole (dots). The photon beam, main electron beam, several tagging electron trajectories (labelled by their energy as a fraction of the main beam energy) and the location of the main focal plane detectors are also indicated.
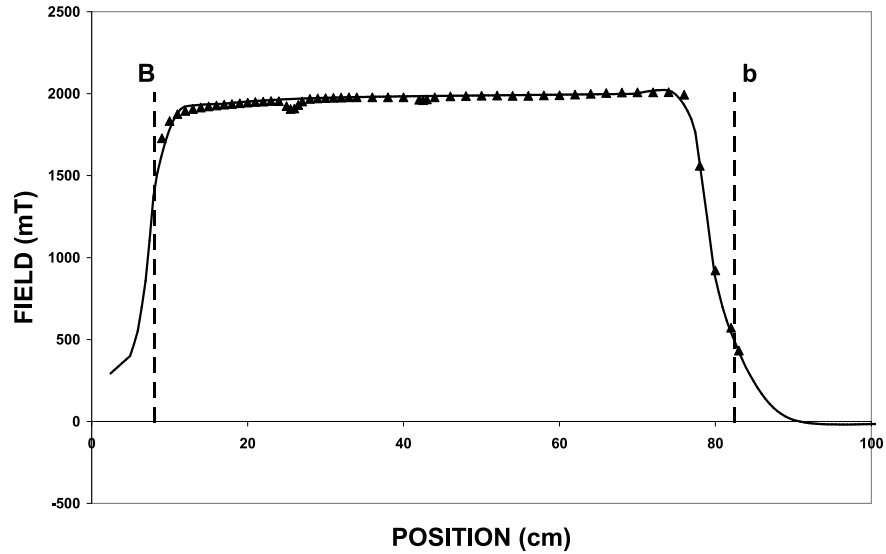
Fig. 3. The magnetic field at 435 A in the upgraded spectrometer measured along line Bb in Fig. 2 compared to the TOSCA prediction (line). The dashed lines show the position of the pole edges.
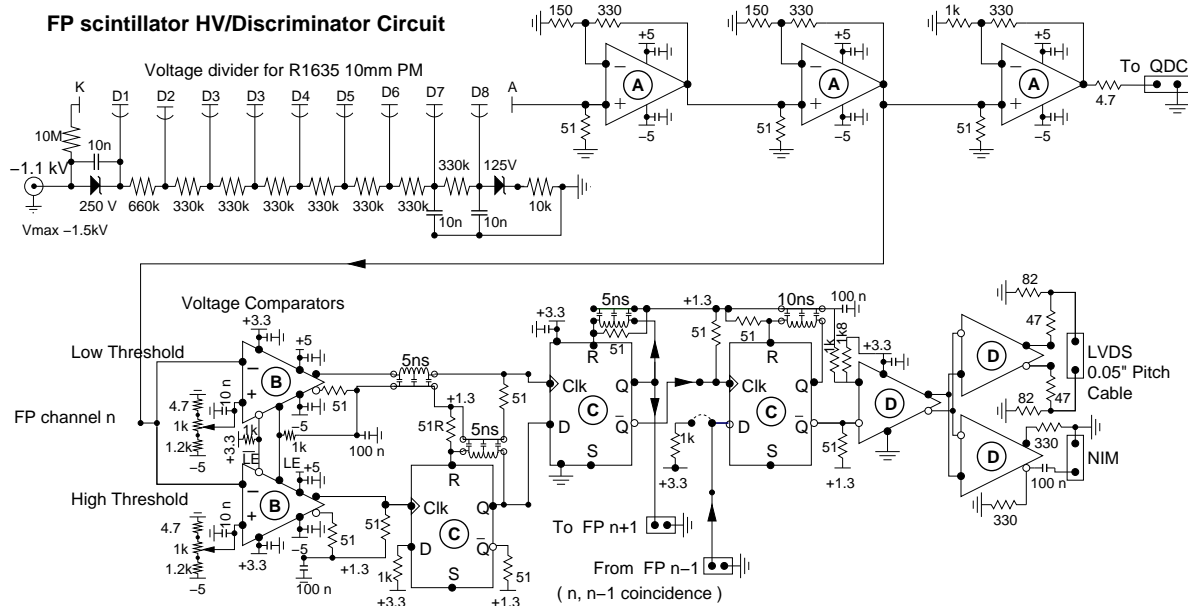
Fig. 4. Circuit diagram of the amplifier-discriminator card. Integrated circuits are labelled A: AD-8009 1 GHz, current-feedback operational amplifier; B: MAX-9601 dual ultrafast comparator; C: MC100LEVL30 triple D-type flip flop with S/R; D: MC100LVEL11 buffer, fan out.
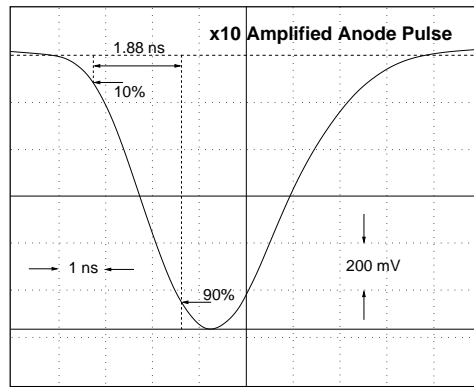
Fig. 5. Amplifier output.
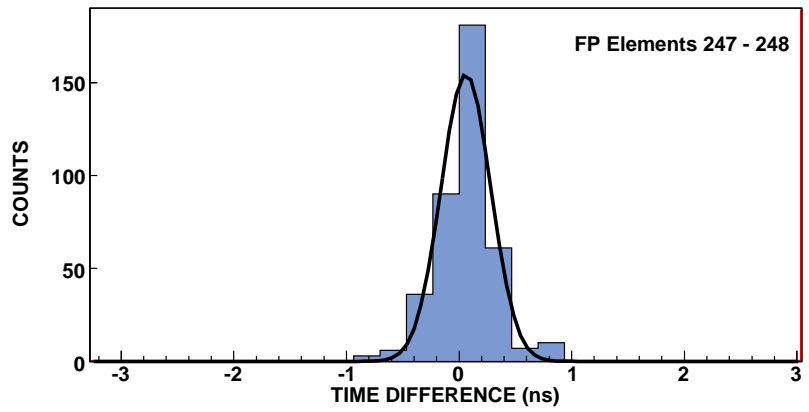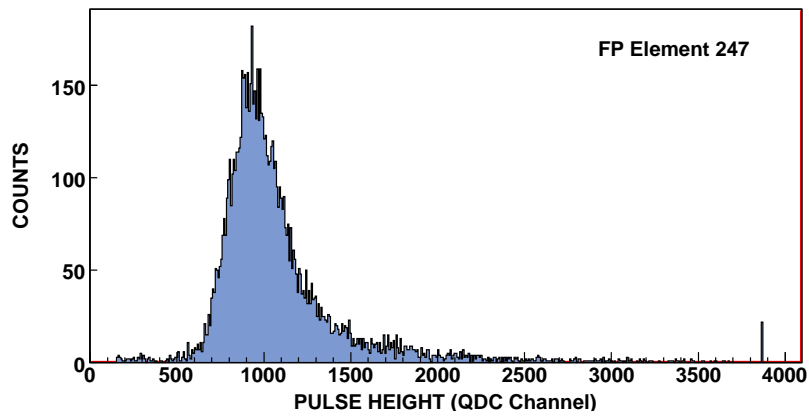

Fig. 6. Focal plane detector performance.
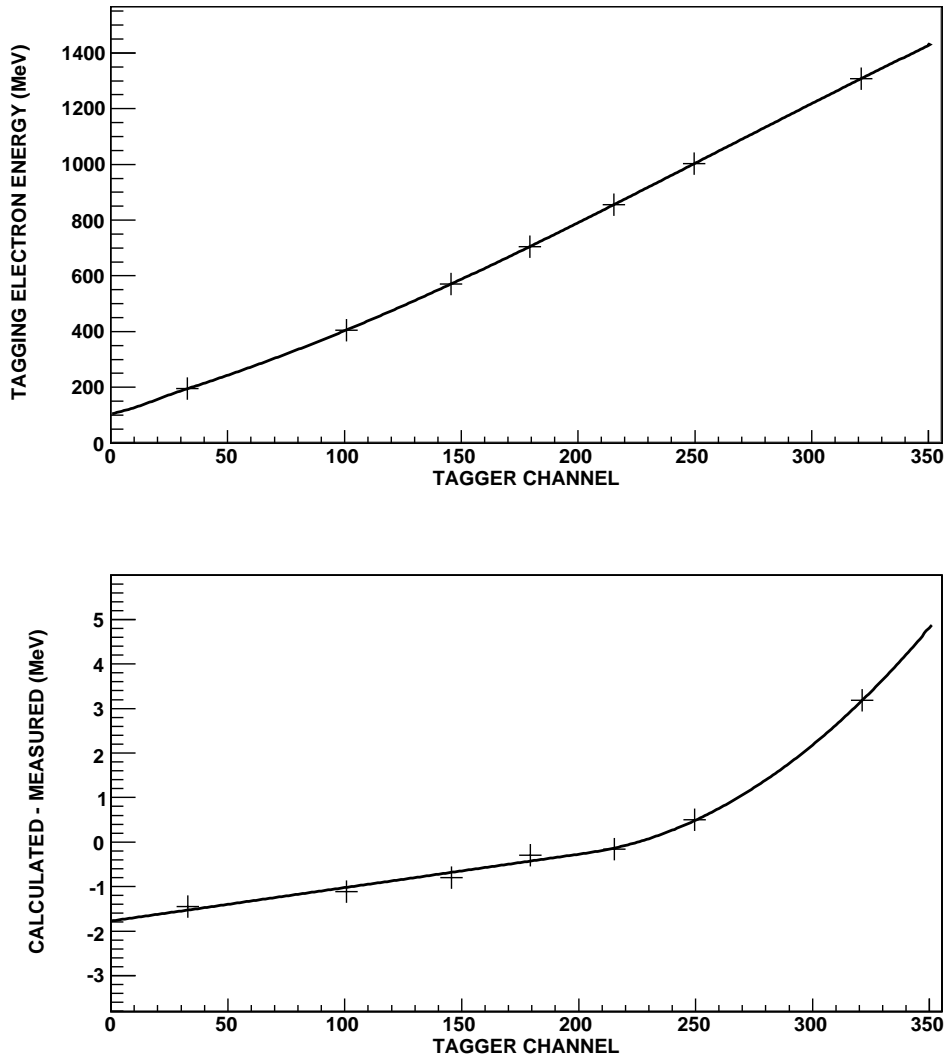
Fig. 7. Upper part: Tagger energy calibration for main beam energy 1508 MeV measured using MAMI energies 195.2, 405.3, 570.3, 705.3, 855.3, 1002.3 and 1307.8 MeV. The line shows the calibration calculated assuming a uniform field.

Lower part: Difference between the calculated and measured calibrations. The line here shows a smooth fit to the seven measured points and indicates the small correction to the calculated calibration required because of large-scale field non-uniformity.
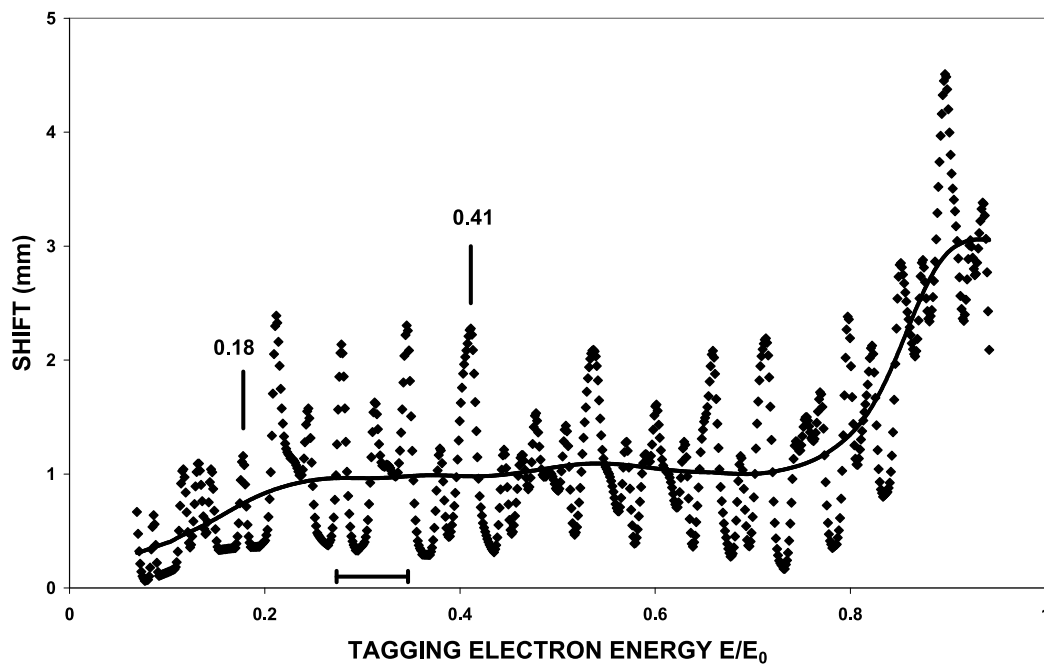
Fig. 8. Calculated shift of the tagging electron trajectories along the focal plane due to the field dips caused by the M8 screws fixing the pole shims. The line is the result of smoothing the points. The horizontal bar shows the region covered by the microscope for the energy calibration data shown in Figs. 9 and 10.
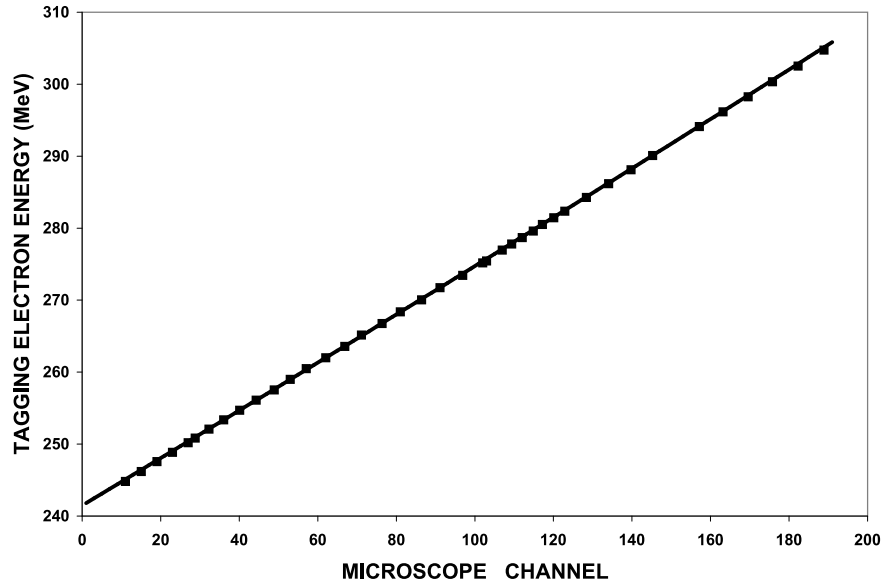
Fig. 9. Energy calibration in the region $E/E_0 = 0.27 - 0.35$ (for $E_0 = 883$ MeV) obtained from scanning a 270.17 MeV beam from MAMI across the microscope by varying the tagger field. The line shows the result of a calculation assuming a uniform field.
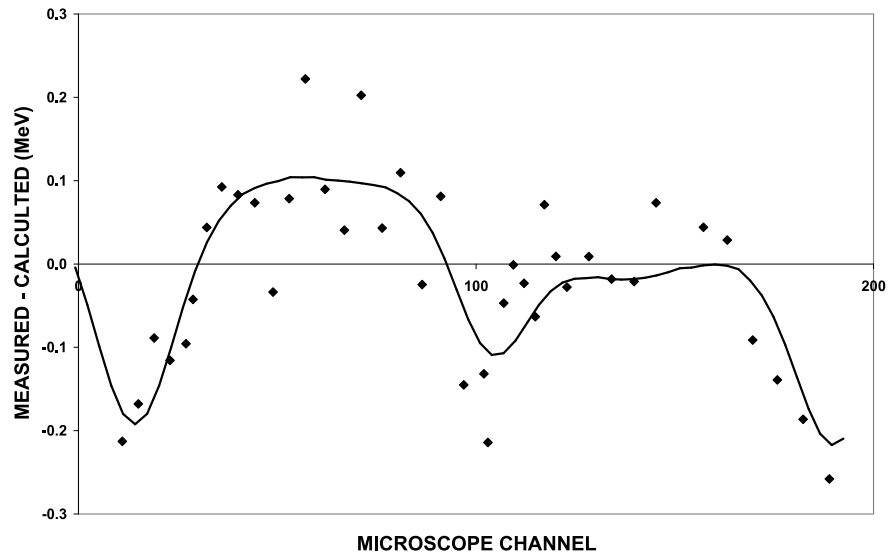
Fig. 10. Difference between the measured and calculated microscope calibrations shown in Fig. 9. The line shows the calculated difference (see text) based on the appropriate section of Fig. 8.
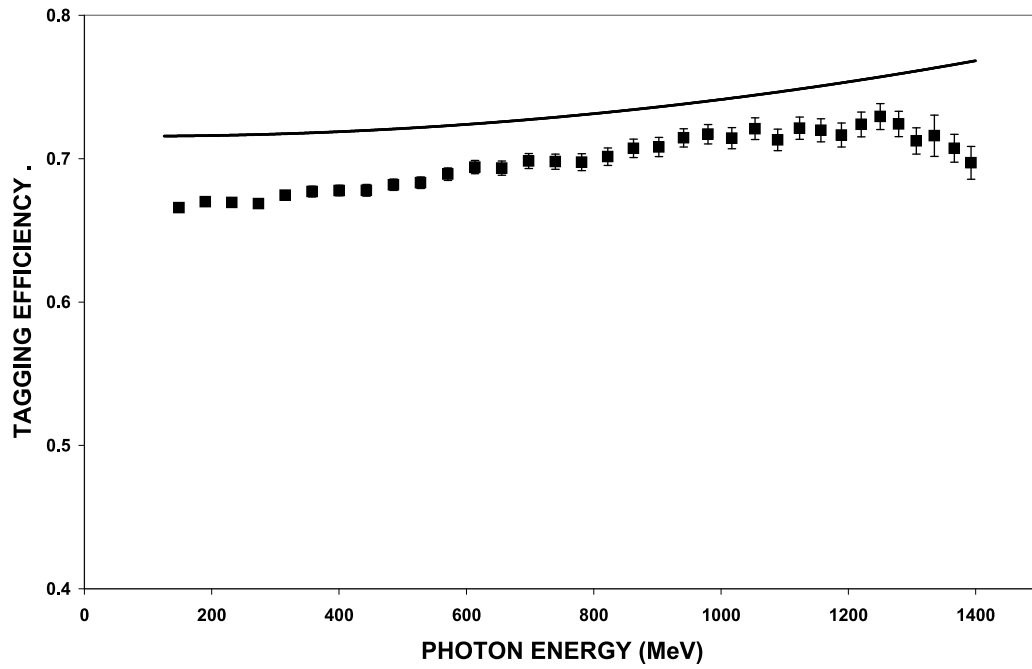
Fig. 11. Tagging efficiency measured at main beam energy of 1508 MeV using a 10 micron thick Cu radiator and a 4 mm diameter collimator. The line shows the result of a Monte Carlo calculation.
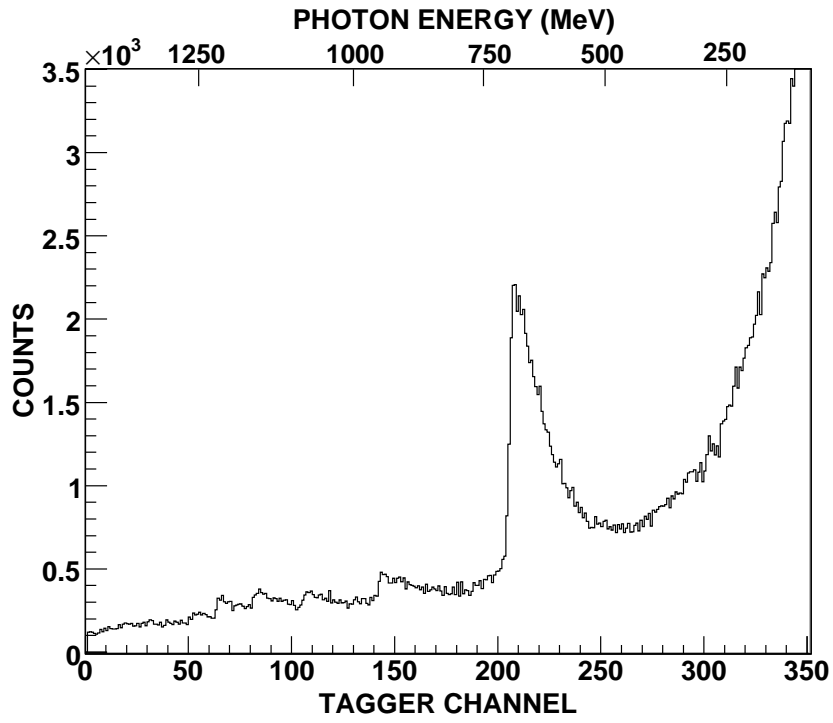
Fig. 12. Tagger spectrum in coincidence with a Pb glass detector placed in the photon beam obtained using a 30 micron thick diamond radiator and a 1 mm diameter collimator.